Parallel Track Initiation for Optical Space Surveillance Using Range and Range-Rate Bounds

Paul W. Schumacher, Jr.
Air Force Research Laboratory, Kihei, Hawaii
Christopher W. T. Roscoe and Matthew P. Wilkins
Applied Defense Solutions, Columbia, Maryland

ABSTRACT

The problem of track initiation is addressed for optical ground or space-based observation of space objects. Angles are the primary quantities available from line-of-sight measurements, but angle rates may also be derived if the data are of sufficient quantity and quality. For a specified rectangular partition in the space of orbital elements, explicit bounds on range and range rate are derived for a given observation based on angles and angle rates. Discretizing the resulting range-range rate hypothesis region allows candidate orbits to be generated in an embarrassingly parallel fashion. The number of hypotheses for track initiation is further constrained by imposing conditions derived from special solutions of Lambert's problem for pairs of observations. Initial results are presented for perfect and noisy simulated data. Also included is an analysis of the sensitivity of the range-range rate bounds with respect to errors in angle rates.

1. INTRODUCTION

The advent of high-sensitivity, high-capacity optical sensors for space surveillance presents us with interesting and challenging tracking problems. Accounting for the origin of every detection made by such systems is generally agreed to belong to the "most difficult" category of tracking problems. Especially in the early phases of the tracking scenario, when a catalog of space objects is being compiled, or when many new objects appear in space because of on-orbit explosion or collision, one faces a combinatorially large number of tracking hypotheses to evaluate. The number of hypotheses is reduced to a more feasible number if observations close together in time can, with high confidence, be associated by the sensor into extended tracks on single objects. Most current space surveillance techniques are predicated on the sensor systems' ability to form such tracks reliably. However, the required operational tempo of space surveillance, the very large number of objects in Earth orbit and the difficulties of detecting dim, fast-moving objects at long ranges mean that individual sensor track reports are often inadequate for computing initial orbit hypotheses. In fact, this situation can occur with optical sensors even when the probability of detection is high. For example, the arc of orbit that has been observed may be too short or may have been sampled too sparsely to allow well-conditioned, usable orbit estimates from single tracks. In that case, one has no choice but to solve a data association problem involving an unknown number of objects and many widely spaced observations of uncertain origin. In the present paper, we are motivated by this more difficult aspect of the satellite cataloging problem. However, the results of this analysis may find use in a variety of less stressing tracking applications.

We begin with the angles-only case, in which angle rate values are not available or are too inaccurate for reliable use. One possible method to deal with such data is to assign a number of range hypotheses to each observation and develop data association hypotheses to be either confirmed or eliminated by comparisons with other data. Assume that we have a pair of line-of-sight unit vectors $\mathbf{u}_1$ and $\mathbf{u}_2$, measured at time t_1 at station position $\mathbf{R}_1$ and time t_2 at station position $\mathbf{R}_2$, respectively (shown schematically in Fig. 1). Assume, without loss of generality, that $t_2 > t_1$. We want to test the hypothesis that these two observations are associated with the same space object. To this end, we attach a set of hypothetical range values, $\{\rho_{1,m}, m = 1,2,...\}$ and $\{\rho_{2,n}, n = 1,2,...\}$ respectively, to each of these measured unit vectors and then generate candidate orbits by solving Lambert's problem for each of the pair-wise combinations of hypothetical orbital position vectors $\mathbf{r}_{1,m}$ and $\mathbf{r}_{2,n}$. Even with a large dataset of measured line-of-sight unit vectors, we can, in principle, consider all possible pairs of observations and solve the family of Lambert problems for each pair. Then each hypothetical orbit from the solution of Lambert's problem is a data association hypothesis that must be either confirmed or eliminated through comparisons with other observational data. This approach allows us to make use of an already proven method (the Search and Determine algorithm and software, SAD) that was designed for generating and testing data association hypotheses for position-type observations typical of radar sensors [1–3]. Given enough range hypotheses for each observed line of sight, we are guaranteed to

Fig. 1. Vector Triangles.

generate a viable candidate orbit for every object that has been observed at two or more distinct times. However, the Cartesian product of the set of range values for each observed line of sight with the sets of range values from every other line of sight implies a possibly prohibitive number of Lambert solutions to generate and check. The computational complexity for generating hypothetical orbits on this approach is quadratic in the number of observed lines of sight and also quadratic in the number of range hypotheses that we attach to the observations.

How should we limit the number of range hypotheses to make the total number of candidate orbits manageable while also generating candidates that are likely to correspond to real orbits of interest? For example, we may be most interested in generating candidate orbits near the geosynchronous equatorial orbital (GEO) belt. Let us seek to generate hypotheses for orbits that lie only in a bounded region of semimajor axis a, eccentricity e, inclination I and right ascension of the ascending node Ω, namely, within a partition specified by the intervals $[a_{\text{MIN}}, a_{\text{MAX}}]$, $[e_{\text{MIN}}, e_{\text{MAX}}]$, $[I_{\text{MIN}}, I_{\text{MAX}}]$ and $[\Omega_{\text{MIN}}, \Omega_{\text{MAX}}]$. (For the purposes of this discussion, we leave the other orbital elements unconstrained. It will turn out that these four elements constrain the possible values of range in simple ways without our having any recourse to angle rate information.) Then, to the extent that we can restrict the generation of hypothetical orbits to a specified partition of the space of orbital elements, we have parallelized the task of building a catalog of objects detected within that partition. The reason is that any partition of the space of orbital elements, including the whole space itself, can be sub-divided into smaller partitions, and each sub-partition can be handled independently. In the approach outlined here, all the observations would have to be considered for each sub-partition of the space of orbit elements. However, by constructing upper and lower bounds on range for each measured line of sight for each sub-partition of the element space, we limit the number of range hypotheses that have to be considered for each sub-partition. This approach allows us to consider a manageable number of range hypotheses for each sub-partition before we generate candidate orbits, simply by making the sub-partitions small enough, so that the overall computation is feasible.

Our emphasis on generating candidate orbits with a Lambert-based approach in the angles-only case is not merely a matter of convenience in extending an existing method such as SAD. Certainly, the bounds on range that we present here could be used in a variety of ways with other angles-based initial orbit determination (IOD) methods. Both the traditional methods of angles-only orbit determination [4] and modern methods such as those of Gooding [5,6] and Karimi and Mortari [7] and others [8] rely on solving for the range by either root-finding or optimization. Such algorithms can always be made to work more reliably when rigorous upper and lower bounds on the unknown quantity are available. However, one encounters at least three difficulties in applying direct angles-only methods to a large, multiple-target catalog-building scenario.

First, although the range bounds presented here allow one to reject candidate solutions based on range, with a direct angles-only method one still has to compute the range in terms of the observations in order to find out if it satisfies the bounds. This turns out to be most of the computation needed to produce the candidate orbits themselves. In the Lambert-based approach, the range bounds allow us to avoid most of the potential computation for the candidate orbits.

Second, the direct angles-only methods do not scale to large problems as well as a Lambert-based method does. Given N observations of line of sight, not necessarily close together in time, the computational load of Lambert-based methods is asymptotically proportional to N^2 (N-choose-2 combinations), because two observations per data association hypothesis are needed. The total computational load of such a method is then proportional to $N^2 M^2$ where M is the number of range hypotheses assigned to each observation. The "constant" of proportionality is itself quadratic in the number of range hypotheses that must be considered for each line of sight. However, as noted above, the latter number can be driven down to manageable size in each partition of the element space by making the partitions small. With traditional methods of angles-only IOD, including that of Gooding [5,6], one faces a

computational load that is asymptotically proportional to N^3 (N-choose-3 combinations), because 3 observations must be associated together to compute the range and hence the candidate orbit. The methods developed by Mortari and Karimi are more robust than traditional methods, but these also require at least 3 observations per association hypothesis. In fact, the approach of Karimi and Mortari [7] works better with more observations per association hypothesis, but then one faces a computational load that scales like N^4, N^5, or even higher. In general, the computational complexity is polynomial in the number of observations, with the polynomial degree equal to the number of observations per data association hypothesis. Of course, it may not be clear in any particular case which approach finally requires fewer processors to achieve a desired production rate of orbit solutions. Higher-degree scaling requires more processors on the traditional range-solution approach and smaller element partitions require more processors on the range-hypothesis approach. The choice may depend on the size and character of the dataset itself and the element partitions of interest.

Third, a Lambert-based method, ideally implemented, will produce a candidate orbit for every real object that has been observed at least twice. In comparison, a direct angles-based method, such as Gooding's, will produce candidate orbits only for those real objects that have been observed at least 3 times. An N^4 method will produce candidate orbits only for those real objects that have been observed at least 4 times, and so on. Hence, the Lambert-based method may do a more complete job of generating viable candidate orbits from real datasets, while scaling more favorably than the direct angles-based methods for large numbers of observations.

The use of angle rate, when it is available, is especially important. If angle rates are available or can be derived from the observation data, a complete orbit hypothesis can be formed for each observation without any iterative solutions, merely by choosing a value of range and a value of range rate. This is the approach outlined by DeMars et al. [9,10]. As in the angles-only case, this track-initiation problem is parallel with respect to element partitions. If we can provide bounds on range and range rate for each element partition, then we can reduce the number of orbit hypotheses needed for each partition simply by making the partitions smaller and using more processors to cover the whole element space. Bounds depending on angle rate will complement the range bounds already available from the angles-only case, and can be expected to further restrict the set of possible range hypotheses.

Most importantly, with accurate angle rate the track initiation job scales linearly with the number of observations rather than as the square or cube, with a computational load proportional to NML if L is the number of range rate hypotheses assigned to each observation. One could hardly expect to do any better than this in solving a large track-initiation problem using optical data. Of course, nothing prevents us from using the improved bounds on range, and possibly range rate, to improve the efficiency of a Lambert-based approach. This choice may depend on whether the angle rates are accurate enough to represent the orbital state directly, or whether they should be used merely to provide extra bounds on the range.

We are seeking explicit bounds on range and possibly range rate that can be applied for each individual angle-based observation, or at most to pairs of angle-based observations. Even with the further restriction that hypothetical orbits be elliptical and Keplerian (which we accept) and even allowing the possibility that the observation may include angle rate values (which we will examine at length), it may not be obvious that efficient bounds having these properties can be obtained. Exact bounds would have to be based on some admissible-region analysis of the type developed by Milani et al. [11], Milani and Knezevic [12], Tommei, Milani, and Rossi [13], Tommei et al. [14], Fujimoto, Maruskin, and Sheeres [15], Farnocchia et al. [16], and Gronchi, Dimare, and Milani [17]. For example, denoting the gravitational parameter by μ, we write the first integrals of Keplerian motion as

$$\text{energy:} \quad E = (\dot{\mathbf{r}} \cdot \dot{\mathbf{r}})/2 - \mu/\|\mathbf{r}\| \tag{1}$$
$$\text{angular momentum:} \quad \mathbf{h} = \mathbf{r} \times \dot{\mathbf{r}} \tag{2}$$
$$\text{Laplace vector:} \quad \mu\mathbf{e} = \dot{\mathbf{r}} \times (\mathbf{r} \times \dot{\mathbf{r}}) - \mu\mathbf{r}/\|\mathbf{r}\| \tag{3}$$

Given the vector triangle relation $\mathbf{r} = \mathbf{R} + \rho\mathbf{u}$ and its time derivative for each observation, we can define admissible regions in the $(\rho, \dot{\rho})$ plane for each partition in the space of elements by means of inequalities such as

$$-\mu/(2a_{\text{MIN}}) \leq E \leq -\mu/(2a_{\text{MAX}}) \tag{4}$$
$$\cos I_{\text{MAX}} \leq (\mathbf{h}/\|\mathbf{h}\|) \cdot \mathbf{k} \leq \cos I_{\text{MIN}} \tag{5}$$
$$e_{\text{MIN}} \leq \|\mathbf{e}\| \leq e_{\text{MAX}} \tag{6}$$

Here **k** is the north polar unit vector in the Earth-centered inertial frame. For each observation, the values of range and range rate that satisfy these inequalities will result in orbits that lie only within the given partition of the space of elements. DeMars and Jah [18] have shown what the admissible regions look like for partitions of semimajor axis and eccentricity by a numerical treatment of the above inequalities. Maruskin, Scheeres, and Alfriend [19] have shown how the admissible regions evolve in time and how the overlap of the admissible regions for different observations can help solve the data association problem. However, even though expressions (1) through (6) can be reduced to polynomial forms in range and range rate, each relation is coupled in both variables and the polynomial degree is high, preventing us from obtaining explicit expressions for range and range rate in terms of the given data. Moreover, the usual admissible-region analysis leads nowhere if angle rates are not available. For example, the track-initiation method of DeMars et al. [9], involving multiple hypotheses on range and range rate, requires both angle and angle rate values. Similarly, the correlation and orbit determination study performed by Milani et al. [20], which used an admissible-region analysis, used simultaneous angle and angle rate data.

In the case where angles are the only observable, it is possible to define a region in the (ρ_1, ρ_2) plane for a pair of observations, analogous to the $(\rho, \dot{\rho})$ admissible region described above. We call this region the range, range admissible region (as opposed to the range, range-rate admissible region). Without explicit closed-form solutions for Lambert's problem, we cannot provide closed-form expressions for the boundaries of the range, range admissible regions. Nevertheless, these regions can be exhibited numerically, and there is plenty of opportunity for future study of the geometrical and topological properties of these regions. In the present analysis, we aim lower and take a simpler geometric and kinematic approach that leads to explicit upper and lower bounds on the possible values of range for each observation or pair of observations, given only angle data at discrete times. In fact, we find several inequalities that must be satisfied simultaneously, and we can take the most restrictive superposition of the different bounds as our working result. In case angle rates are available, we can find additional bounding regions in the range, range rate plane. It may happen that, for a given observation, there are no values of the range or range rate that lead to orbits within the given element-space partition, so that the observation can be eliminated from further consideration. We obtain explicit conditions for the existence of possible values of range and range rate in terms of the observation itself.

The price for obtaining explicit bounds on range is that the bounds are not exact but somewhat conservative. We call the region defined by these bounds the range, range hypothesis region. We construct it so that it always contains the exact range, range admissible region. Although every orbit within the element-space partition corresponds to values of range that lie within the bounds given here, some values of range that satisfy the bounds may lead to orbits that lie outside the given partition. Naturally, similar statements hold for the more usual range, range rate admissible regions and their corresponding hypothesis regions. The situation is shown schematically in Fig. 2.

This circumstance represents inefficiency in the parallelization of building the catalog: nearly the same candidate orbits near the boundaries of the element-space partitions may be generated in both of the adjacent partitions, if the range or range rate hypotheses are planted densely enough. How to sample the hypothesis regions is, in fact, still an open question for hypothesis methods such as this: typical approaches use either a rectangular grid or a Delaunay triangulation [13], but an alternate approach using an iso-energy grid has been suggested recently by Siminski et al. [21,22] In any case, no candidate orbits within the given element-space partitions will be missed because of the bounds given here. The extent and cost of the inefficient duplication of candidate orbits will depend on the particular datasets and element partitions of interest, and may require further study if the tracking scenario is computationally
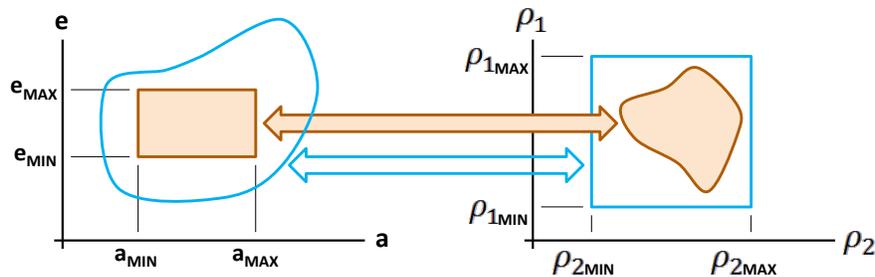
Fig. 2. Relationship between hypothesis region (blue) and admissible region (orange).

stressing. In practice, of course, within any element partition, any of these extra orbit hypotheses can be either kept or discarded. If they are kept, we would have, at most, a bookkeeping problem of transferring the extra orbit solutions to the correct element partition. The trade-off in this case is that merely moving data between processors always takes time. We note also that each candidate orbit is used in exactly the same way, and the overall tracking job proceeds in the same way, regardless of whether any candidate orbits happen to originate in the "wrong" element partition, as long as all observations are available to each processor.

2. BOUNDS ON RANGE IMPLIED BY ANGLE VALUES

Here we present bounds on range that must hold for each observed line of sight. Assuming that all orbits of interest are elliptical, require that the orbital radii lie between the maximum specified apogee and the minimum specified perigee:

$$[a_{\text{MIN}}(1 - e_{\text{MAX}})]^2 \leq \|\mathbf{r}\|^2 \leq [a_{\text{MAX}}(1 + e_{\text{MAX}})]^2 \tag{7}$$

The values of range that correspond to these limits on orbital radius can be found explicitly using the vector triangle relationship $\mathbf{r} = \mathbf{R} + \rho\mathbf{u}$. Squaring terms to remove the radical, we have

$$a_{\text{MIN}}^2(1 - e_{\text{MAX}})^2 \leq \mathbf{R} \cdot \mathbf{R} + 2(\mathbf{R} \cdot \mathbf{u})\rho + \rho^2 \leq a_{MAX}^2(1 + e_{\text{MAX}})^2 \tag{8}$$

Consider the perigee and apogee cases separately. For the perigee case, we require the orbital radius to be no smaller than the smallest allowable perigee radius:

$$a_{\text{MIN}}^2(1 - e_{\text{MAX}})^2 \leq \mathbf{R} \cdot \mathbf{R} + 2(\mathbf{R} \cdot \mathbf{u})\rho + \rho^2 \tag{9}$$
$$\rho^2 + 2(\mathbf{R} \cdot \mathbf{u})\rho - [a_{\text{MIN}}^2(1 - e_{\text{MAX}})^2 - \mathbf{R} \cdot \mathbf{R}] \geq 0 \tag{10}$$

The roots of this quadratic are:

$$\rho = -(\mathbf{R} \cdot \mathbf{u}) \pm \sqrt{(\mathbf{R} \cdot \mathbf{u})^2 + [a_{\text{MIN}}^2(1 - e_{\text{MAX}})^2 - \mathbf{R} \cdot \mathbf{R}]} \tag{11}$$

We will have real roots if and only if the argument of the square root is non-negative:

$$a_{\text{MIN}}^2(1 - e_{\text{MAX}})^2 \geq \mathbf{R} \cdot [\mathbf{R} - (\mathbf{R} \cdot \mathbf{u})\mathbf{u}] \tag{12}$$

If no real roots of the quadratic expression (10) exist, then we can immediately discard the current observation and form no hypotheses with it. The reason is that no value of the range will be found for this observation, which is consistent with the specified intervals of the orbital elements.

Descartes' rule of signs tells us the number of positive real roots. If the third coefficient in the quadratic form (10) is negative, that is, if $a_{\text{MIN}}^2(1 - e_{\text{MAX}})^2 > \mathbf{R} \cdot \mathbf{R}$, then, regardless of the sign of the second coefficient $2(\mathbf{R} \cdot \mathbf{u})$, we will have one positive real root and necessarily also one negative root. Because the quadratic is concave-up, the inequality is satisfied to the left of the negative root and to the right of the positive root. We can ignore the negative root and all values to the left of it, because we require *a priori* that range values to be non-negative. What remains is a positive lower limit on the possible values of range:

$$\rho \geq -(\mathbf{R} \cdot \mathbf{u}) + \sqrt{(\mathbf{R} \cdot \mathbf{u})^2 + [a_{\text{MIN}}^2(1 - e_{\text{MAX}})^2 - \mathbf{R} \cdot \mathbf{R}]} \tag{13}$$

It is worth noting that, for Earth-bound stations, the third coefficient of (10) will essentially always be negative because the inequality $a_{\text{MIN}}^2(1 - e_{\text{MAX}})^2 > \mathbf{R} \cdot \mathbf{R}$ is approximately the condition that the minimum allowable perigee radius be larger than the Earth radius. Moreover, the second coefficient $2(\mathbf{R} \cdot \mathbf{u})$ will essentially always be positive because observations have to be taken above the local horizontal plane at some positive local elevation angle. For space-based observing stations, it is possible that neither of these circumstances would be true: the station's orbital position may be higher than the minimum specified perigee radius, or observations may be taken at negative local elevation angles, or both.

If the third coefficient in (10) is positive, that is, if $a_{\text{MIN}}^2(1 - e_{\text{MAX}})^2 < \mathbf{R} \cdot \mathbf{R}$, then the quadratic will have either no positive real roots or two positive real roots, depending on the sign of the second coefficient. This is the possibility just mentioned for space-based stations, although we do not expect this possibility for Earth-bound stations unless

we are interested in orbits with perigee radii less than the Earth radius. If, furthermore, the second coefficient in (10) is positive, that is, if $(\mathbf{R} \cdot \mathbf{u}) > 0$, then we have no positive real roots, but only a pair of negative roots. Because the quadratic is concave-up, the inequality (10) is satisfied to the left of the more negative root and to the right of the less negative root. However, since we require *a priori* that range values be non-negative, we are left merely with the condition that $\rho \geq 0$. If the second coefficient is negative, that is, $(\mathbf{R} \cdot \mathbf{u}) < 0$, meaning that the observation is taken at negative local elevation angle, then the quadratic will have two positive real roots. Because the quadratic is concave-up, the inequality (10) will be satisfied to the left of the smaller root, that is, between $\rho = 0$ and the smaller root, and also to the right of the larger root. In this case, we have two disjoint intervals of range, one finite and one semi-infinite, over which range hypotheses will satisfy the perigee constraint:

$$0 \leq \rho \leq -(\mathbf{R} \cdot \mathbf{u}) - \sqrt{(\mathbf{R} \cdot \mathbf{u})^2 + [a_{\text{MIN}}^2(1 - e_{\text{MAX}})^2 - \mathbf{R} \cdot \mathbf{R}]} \tag{14}$$

$$\rho \geq -(\mathbf{R} \cdot \mathbf{u}) + \sqrt{(\mathbf{R} \cdot \mathbf{u})^2 + [a_{\text{MIN}}^2(1 - e_{\text{MAX}})^2 - \mathbf{R} \cdot \mathbf{R}]} \tag{15}$$

Now we consider the apogee case and seek to derive results that are analogous to those above. The apogee case will provide us with conditions on values of the range that are complementary to those of the perigee case. Since both sets of conditions must be satisfied simultaneously, we can take the most restrictive superposition of all conditions on range to define the set of values over which to form range hypotheses.

For the apogee case, we have from the inequality (8) that the orbital radius must be no larger than the maximum allowable apogee radius:

$$\mathbf{R} \cdot \mathbf{R} + 2(\mathbf{R} \cdot \mathbf{u})\rho + \rho^2 \leq a_{MAX}^2(1 + e_{\text{MAX}})^2 \tag{16}$$
$$\rho^2 + 2(\mathbf{R} \cdot \mathbf{u})\rho - [a_{MAX}^2(1 + e_{\text{MAX}})^2 - \mathbf{R} \cdot \mathbf{R}] \leq 0 \tag{17}$$

The roots are:

$$\rho = -(\mathbf{R} \cdot \mathbf{u}) \pm \sqrt{(\mathbf{R} \cdot \mathbf{u})^2 + [a_{MAX}^2(1 + e_{\text{MAX}})^2 - \mathbf{R} \cdot \mathbf{R}]} \tag{18}$$

We will have real roots if and only if the argument of the square root is non-negative:

$$a_{MAX}^2(1 + e_{\text{MAX}})^2 \geq \mathbf{R} \cdot [\mathbf{R} - (\mathbf{R} \cdot \mathbf{u})\mathbf{u}] \tag{19}$$

If no real roots exist, then we can immediately discard the observation and form no hypotheses with it. The reason is that no value of the range will be found for this observation, which is also consistent with the specified intervals of the orbital elements.

Assuming that we have real roots in equation (18), we use Descartes' rule of signs to determine the number of positive real roots. If the third coefficient in the quadratic form (17) is negative, that is, if $a_{MAX}^2(1 + e_{\text{MAX}})^2 > \mathbf{R} \cdot \mathbf{R}$, then, regardless of the sign of the second coefficient $2(\mathbf{R} \cdot \mathbf{u})$, we will have one positive real root and necessarily also one negative root. Because the quadratic is concave-up, the inequality (17) is satisfied between the roots. Moreover, we require *a priori* that range values be non-negative, so we can say without loss of generality that the inequality will be satisfied between $\rho = 0$ and the positive real root. The result is that we have an upper bound on the possible values of range:

$$0 \leq \rho \leq -(\mathbf{R} \cdot \mathbf{u}) + \sqrt{(\mathbf{R} \cdot \mathbf{u})^2 + [a_{MAX}^2(1 + e_{\text{MAX}})^2 - \mathbf{R} \cdot \mathbf{R}]} \tag{20}$$

It is worth noting that, for Earth-bound stations, the third coefficient will essentially always be negative because the inequality $a_{MAX}^2(1 + e_{\text{MAX}})^2 > \mathbf{R} \cdot \mathbf{R}$ is approximately the condition that the maximum allowable apogee radius be larger than the Earth radius. Moreover, the second coefficient $2(\mathbf{R} \cdot \mathbf{u})$ will essentially always be positive because observations have to be taken above the local horizontal plane at some positive local elevation angle. For space-based observing stations, it is possible that neither of these circumstances would be true: the station's orbital position may be above the maximum specified apogee radius, or observations may be taken at negative local elevation angles, or both.

If the third coefficient in (17) is positive, that is, if $a_{MAX}^2(1 + e_{MAX})^2 < \mathbf{R} \cdot \mathbf{R}$, then the quadratic will have either no positive real roots or two positive real roots, depending on the sign of the second coefficient. This is the possibility just mentioned for space-based stations, although we do not expect this case for Earth-bound stations. If, furthermore, the second coefficient in (17) is positive, that is, if $(\mathbf{R} \cdot \mathbf{u}) > 0$, then we have no positive real roots, but only a pair of negative roots. Because the quadratic is concave-up, the inequality (17) is satisfied between these roots. However, since we require *a priori* that range values be non-negative, we can discard this particular observation and form no range hypotheses for it.

If the third coefficient in (17) is positive, but the second coefficient is negative, $(\mathbf{R} \cdot \mathbf{u}) < 0$, meaning that the observation is taken at negative local elevation angle, then the quadratic will have two positive real roots. The quadratic is concave-up, so the inequality (17) will be satisfied between these two roots. In this case, we have a single finite interval of range over which range hypotheses will satisfy the apogee condition:

$$\rho \geq -(\mathbf{R} \cdot \mathbf{u}) - \sqrt{(\mathbf{R} \cdot \mathbf{u})^2 + [a_{MAX}^2(1 + e_{MAX})^2 - \mathbf{R} \cdot \mathbf{R}]} \tag{21}$$

$$\rho \leq -(\mathbf{R} \cdot \mathbf{u}) + \sqrt{(\mathbf{R} \cdot \mathbf{u})^2 + [a_{MAX}^2(1 + e_{MAX})^2 - \mathbf{R} \cdot \mathbf{R}]} \tag{22}$$

The set of range values over which we may have to form hypotheses for the observation in question is given by the intersection of all of the above conditions, both for perigee and apogee cases.

3. RESTRICTIONS IMPLIED BY THE SET OF ORBITAL PLANES

The above conditions are bounds on the possible values of range, which can be computed for each single observation. The fact that only single observations are involved is what allows us to find explicit bounds for each of the ranges before we form any range hypotheses. However, additional restrictions on the allowable values of range can be deduced from relations that involve both of the ranges presented for a solution to Lambert's problem. Although the nonlinearities in these relations prevent us from getting explicit inequalities, nevertheless we can formulate additional conditions that ρ_1 and ρ_2 must satisfy. Checking these extra conditions for each range pair may keep us from having to produce some unnecessary and expensive Lambert solutions.

Using the vector triangle relation $\mathbf{r} = \mathbf{R} + \rho\mathbf{u}$ for each of the two lines of sight, compute the unit vector $\mathbf{n}$ normal to the candidate orbital plane:

$$\mathbf{n} = s\,(\mathbf{r}_1 \times \mathbf{r}_2)/\|\mathbf{r}_1 \times \mathbf{r}_2\| \tag{23}$$

Here the quantity s is a signum function: $s = +1$ for "short-way" trajectories and $s = -1$ for "long-way" trajectories. In general, we do not know *a priori* the sign for s and both cases will need to be considered. With the sign chosen, the inclination is given unambiguously by

$$\cos I = \mathbf{n} \cdot \mathbf{k} \tag{24}$$

Hence we require that

$$\cos I_{MAX} \leq \mathbf{n} \cdot \mathbf{k} \leq \cos I_{MIN} \tag{25}$$

In the case of low-inclination intervals, it may be better to work in terms of sine inclination:

$$\sin I_{MIN} \leq \sqrt{1 - (\mathbf{n} \cdot \mathbf{k})^2} \leq \sin I_{MAX} \tag{26}$$

In a similar way, we use the unit nodal vector to obtain conditions that the range pair must satisfy if the candidate orbit is to lie within a specified interval of right ascension of the ascending node, $[\Omega_{MIN}, \Omega_{MAX}]$. In the Earth-centered inertial frame, we have

$$(\mathbf{k} \times \mathbf{n})/\|\mathbf{k} \times \mathbf{n}\| = (\cos\Omega, \sin\Omega, 0)^T \tag{27}$$

so that, following standard logic for quadrant resolution, we require

$$\Omega_{MIN} \leq \tan^{-1}(\sin\Omega/\cos\Omega) \leq \Omega_{MAX} \tag{28}$$

Of course, for important special cases like near-GEO orbits, it may be preferable to define partitions in terms of nonsingular elements such as $p \triangleq \sin(I/2)\cos\Omega$ and $q \triangleq \sin(I/2)\sin\Omega$. No special difficulty attaches to working with these or any other elements related to the orbit plane.

4. RESTRICTIONS IMPLIED BY LAMBERT'S THEOREM

Next, we can use three special solutions of Lambert's problem to restrict the ranges. The eccentricity of the orbit of least possible eccentricity that goes through a given pair of position vectors can be computed solely in terms of those position vectors. Call it e_0. Likewise, the semimajor axis of the orbit of least possible semimajor axis that goes through the pair of positions can be computed solely in terms of the position vectors. Call it a_0. The formulas for a_0 and e_0 are well known:

$$4a_0 = \|\mathbf{r}_1\| + \|\mathbf{r}_2\| + \|\mathbf{r}_2 - \mathbf{r}_1\| \quad \text{and} \quad e_0 = \frac{|(\|\mathbf{r}_1\| - \|\mathbf{r}_2\|)|}{\|\mathbf{r}_2 - \mathbf{r}_1\|} \tag{29}$$

Hence, for each hypothesized range pair (ρ_1, ρ_2), we compute the corresponding position vectors and apply the following logic:

> If $a_0 > a_{MAX}$, then reject the hypothesis pair without solving Lambert's problem, because the geometry is guaranteed to produce a larger semimajor axis than specified.

> If $e_0 > e_{MAX}$, then reject the hypothesis pair without solving Lambert's problem, because the geometry is guaranteed to produce a larger eccentricity than specified.

Of course, even for a (ρ_1, ρ_2) hypothesis that passes all of the above tests, the actual solution of Lambert's problem may still turn out to get rejected once we have computed the elements of the candidate orbit. The reason is that none of the conditions on range derived so far involves the minimum allowable eccentricity, e_{MIN}. This fundamental feature of our problem raises the question of how well we can limit the generation of candidate orbits to lie within the given eccentricity interval. Let us assume that the hypothetical range pair is not rejected by the above criterion, so that $e_0 \leq e_{MAX}$. Assume also that all of the range bounds and other conditions that depend on single observations have already been applied. Then we know that the Lambert solution for a pair of range hypotheses will not produce an orbit having eccentricity outside the interval $[e_0, e_{MAX}]$. If $e_{MIN} \leq e_0$, we have no difficulty: the candidate orbit will have an eccentricity within the given interval $[e_{MIN}, e_{MAX}]$. However, if $e_0 < e_{MIN}$, then the eccentricity of the candidate orbit may or may not lie within the specified interval. The Lambert solution has to be generated and then either kept if the eccentricity is at least as large as e_{MIN} or discarded if the candidate eccentricity turns out to be less than e_{MIN}. As noted previously, this represents some inefficiency in the generation of candidate orbits, especially if nearly those same candidate orbits were to be generated in the processing for other element-space partitions. The extent of the overall inefficiency depends on the dataset and the actual element-space partitions being used, so we cannot draw general conclusions. It would be helpful at this point to have reasonably sharp bounds on the actual eccentricity in the Lambert problem without having to solve the whole problem. However, lacking that, we have no better recourse than to generate the candidate orbit. Overall, we do expect to be able to reduce the number of Lambert solutions that have to be generated, compared to the number required without the above checks involving a_0 and e_0.

Next, consider Euler's Theorem, a special case of Lambert's Theorem, which expresses the time of flight Δt_P between given position vectors on a parabolic (zero-energy) orbit:

$$\Delta t_P = \frac{4}{3}\sqrt{a_0^3/\mu}\,(1 - s\,\lambda^3) \tag{30}$$

Again, the quantity s is a signum function: $s = +1$ for "short-way" trajectories and $s = -1$ for "long-way" trajectories. The parameter λ is defined in terms of the position vectors:

$$0 \leq \lambda^2 = \frac{\|\mathbf{r}_1\| + \|\mathbf{r}_2\| - \|\mathbf{r}_2 - \mathbf{r}_1\|}{\|\mathbf{r}_1\| + \|\mathbf{r}_2\| + \|\mathbf{r}_2 - \mathbf{r}_1\|} \leq 1 \tag{31}$$

Because, for given position vectors, the time of flight in Lambert's problem is a monotonic decreasing function of the orbital energy, elliptic (negative-energy) orbits will always have a time of flight longer than the parabolic time, and hyperbolic (positive-energy) orbits will always have a time of flight shorter than the parabolic time. In our case, we can require that our observation pairs and range hypotheses always produce elliptic orbits:

$$t_2 - t_1 > \Delta t_P \tag{32}$$

Combinations that do not satisfy this condition can be eliminated without generating a Lambert solution.

Finally, the solution of Lambert's problem for elliptic orbits requires us to specify the number of complete orbital revolutions, N_{REV} , between the initial and final times. We cannot have an arbitrarily large number of revolutions in the given time of flight because the period of the orbit of minimum possible period T_0 is fixed by the geometry of the problem:

$$T_0 = 2\pi \sqrt{a_0^3/\mu} \tag{33}$$

Accounting for the fact that some fraction of a revolution must remain after N_{REV} complete revolutions on the solution orbit, including possibly zero complete revolutions, the time of flight and number of revolutions must satisfy the inequality

$$t_2 - t_1 \geq N_{\text{REV}} T \tag{34}$$

where T is the actual period. Without solving Lambert's problem, we do not know T . However, it is always true that the period is at least equal to T_0 . Hence the time of flight must also satisfy the inequality

$$t_2 - t_1 \geq N_{\text{REV}} T_0 = 2\pi N_{\text{REV}} \sqrt{a_0^3/\mu} \tag{35}$$

Because of the unknown difference between T and T_0 , it is possible that the number of complete revolutions allowed by inequality (35) is larger than the true maximum number of revolutions allowed in solutions of Lambert's problem.

Given an observation pair $\mathbf{u}_1$ and $\mathbf{u}_2$, the previous formulas and the associated logic can be used to decide if a hypothetical pair of ranges should be used to generate a Lambert solution. Of course, whatever Lambert solutions are generated should be verified for compliance with the specified interval of eccentricity, because none of the conditions on range derived so far depends on the value of the minimum allowable eccentricity e_{MIN} .

5. BOUNDS ON RANGE AND RANGE RATE IMPLIED BY SIMULTANEOUS ANGLES AND ANGLE RATES

In case the observations include, or allow us to derive, angle rates, we can deduce additional bounds on the possible values of range. Like the bounds derived above from perigee and apogee distances, these extra bounds will apply to single observations, where we now understand an observation to consist of the values $\left(\mathbf{R}, \dot{\mathbf{R}}, \mathbf{u}, \dot{\mathbf{u}}\right)$ at a known time. Differentiating the vector triangle relation $\mathbf{r} = \mathbf{R} + \rho\mathbf{u}$, we get the orbital velocity:

$$\dot{\mathbf{r}} = \dot{\mathbf{R}} + \dot{\rho}\mathbf{u} + \rho\dot{\mathbf{u}} \tag{36}$$

With the observational data given, the speed of the object is a function of only two variables:

$$f(\rho, \dot{\rho}) \triangleq (\dot{\mathbf{r}} \cdot \dot{\mathbf{r}}) = \dot{\mathbf{R}} \cdot \dot{\mathbf{R}} + 2\dot{\rho}\dot{\mathbf{R}} \cdot \mathbf{u} + 2\rho\dot{\mathbf{R}} \cdot \dot{\mathbf{u}} + \dot{\rho}^2 + \rho^2\,\dot{\mathbf{u}} \cdot \dot{\mathbf{u}} \tag{37}$$

which has no terms containing both range and range rate. It is worth noting that if we happen to have zero apparent angular rate at the moment of an observation, that is, if $\dot{\mathbf{u}} = \mathbf{0}$, then $f(\rho, \dot{\rho})$ is independent of range at that moment. This situation means that apparent angular rate does not restrict the range at that moment, although some restriction on range rate must still exist.

We require the velocity magnitude to lie between the minimum possible apogee speed and the maximum possible perigee speed:

$$\frac{\mu}{a_{\text{MAX}}}\left(\frac{1-e_{\text{MAX}}}{1+e_{\text{MAX}}}\right) \leq \|\dot{\mathbf{r}}\|^2 \leq \frac{\mu}{a_{\text{MIN}}}\left(\frac{1+e_{\text{MAX}}}{1-e_{\text{MAX}}}\right) \tag{38}$$

We are looking for the region in the $(\rho, \dot{\rho})$ plane implied by these inequalities. We define this region by the set-intersection of the intervals of range and range rate corresponding to each of the two inequalities.

5.1 Perigee Speed Case

Consider the perigee case first.

$$f(\rho, \dot{\rho}) \leq \frac{\mu}{a_{\text{MIN}}}\left(\frac{1+e_{\text{MAX}}}{1-e_{\text{MAX}}}\right) \tag{39}$$

$$\dot{\mathbf{R}}\cdot\dot{\mathbf{R}} + 2\dot{\rho}\dot{\mathbf{R}}\cdot\mathbf{u} + 2\rho\dot{\mathbf{R}}\cdot\dot{\mathbf{u}} + \dot{\rho}^2 + \rho^2\,\dot{\mathbf{u}}\cdot\dot{\mathbf{u}} - \frac{\mu}{a_{\text{MIN}}}\left(\frac{1+e_{\text{MAX}}}{1-e_{\text{MAX}}}\right) \leq 0 \tag{40}$$

To define this region explicitly in terms of one of the variables, we can solve this inequality either for range rate in terms of range or range in terms of range rate. The two choices lead to exactly equivalent results because the level curves of the quadratic function (37) are ellipses. In this paper, we choose to solve for range rate in terms of range.

$$\dot{\rho}^2 + 2\dot{\rho}\dot{\mathbf{R}}\cdot\mathbf{u} + \rho^2\,\dot{\mathbf{u}}\cdot\dot{\mathbf{u}} + 2\rho\dot{\mathbf{R}}\cdot\dot{\mathbf{u}} + \dot{\mathbf{R}}\cdot\dot{\mathbf{R}} - \frac{\mu}{a_{\text{MIN}}}\left(\frac{1+e_{\text{MAX}}}{1-e_{\text{MAX}}}\right) \leq 0 \tag{41}$$

The roots are

$$\dot{\rho} = -\dot{\mathbf{R}}\cdot\mathbf{u} \pm \sqrt{\left(\dot{\mathbf{R}}\cdot\mathbf{u}\right)^2 - \left[\rho^2\,\dot{\mathbf{u}}\cdot\dot{\mathbf{u}} + 2\rho\dot{\mathbf{R}}\cdot\dot{\mathbf{u}} + \dot{\mathbf{R}}\cdot\dot{\mathbf{R}} - \frac{\mu}{a_{\text{MIN}}}\left(\frac{1+e_{\text{MAX}}}{1-e_{\text{MAX}}}\right)\right]} \tag{42}$$

Provided that we have real roots for $\dot{\rho}$, the inequality (41) will be satisfied between the roots because the quadratic form in range rate is concave-up. Obviously, real roots for range rate exist if and only if the argument of the square root is non-negative, but now this condition depends on the range:

$$\left(\dot{\mathbf{R}}\cdot\mathbf{u}\right)^2 - \left[\rho^2\,\dot{\mathbf{u}}\cdot\dot{\mathbf{u}} + 2\rho\dot{\mathbf{R}}\cdot\dot{\mathbf{u}} + \dot{\mathbf{R}}\cdot\dot{\mathbf{R}} - \frac{\mu}{a_{\text{MIN}}}\left(\frac{1+e_{\text{MAX}}}{1-e_{\text{MAX}}}\right)\right] \geq 0 \tag{43}$$

$$\rho^2\,\dot{\mathbf{u}}\cdot\dot{\mathbf{u}} + 2\rho\dot{\mathbf{R}}\cdot\dot{\mathbf{u}} + \left[f^* - \frac{\mu}{a_{\text{MIN}}}\left(\frac{1+e_{\text{MAX}}}{1-e_{\text{MAX}}}\right)\right] \leq 0 \tag{44}$$

where the quantity f^* is defined as

$$f^* = \dot{\mathbf{R}}\cdot\dot{\mathbf{R}} - \left(\dot{\mathbf{R}}\cdot\mathbf{u}\right)^2 \tag{45}$$

If the equality in (44) has no real roots, then we can eliminate the observation and form no hypotheses with it. The reason is that no real value of the range can be found that will lead to real values for range rate. If the equality in (44) has real roots, then the inequality, being concave-up, is satisfied for all values of range between the roots, and these values of range lead to real values of range rate, according to (42) above. Of course, we also require that the range be non-negative, which further restricts the values of range rate allowed by (41).

As an aside, we note that, if $\|\dot{\mathbf{u}}\| = 0$, then, independently of the value of range, the inequality (44) reduces to

$$f^* \leq \frac{\mu}{a_{\text{MIN}}}\left(\frac{1+e_{\text{MAX}}}{1-e_{\text{MAX}}}\right) \tag{46}$$

Therefore, in the special case of zero total angular rate, we may eliminate the observation if (46) is not satisfied, because, in that case, no real values for range rate are possible. If the total angular rate is zero, but (46) is satisfied, then the inequality (41) reduces to an expression involving range rate but not range:

$$\dot{\rho}^2 + 2\dot{\rho}\dot{\mathbf{R}}\cdot\mathbf{u} + \dot{\mathbf{R}}\cdot\dot{\mathbf{R}} - \frac{\mu}{a_{\text{MIN}}}\left(\frac{1+e_{\text{MAX}}}{1-e_{\text{MAX}}}\right) \leq 0 \tag{47}$$

The roots in this case are real and reduce to

$$\dot{\rho} = -\dot{\mathbf{R}} \cdot \mathbf{u} \pm \sqrt{\left(\dot{\mathbf{R}} \cdot \mathbf{u}\right)^2 - \left[\dot{\mathbf{R}} \cdot \dot{\mathbf{R}} - \frac{\mu}{a_{MIN}}\left(\frac{1 + e_{MAX}}{1 - e_{MAX}}\right)\right]} \tag{48}$$

$$\dot{\rho} = -\dot{\mathbf{R}} \cdot \mathbf{u} \pm \sqrt{\frac{\mu}{a_{MIN}}\left(\frac{1 + e_{MAX}}{1 - e_{MAX}}\right) - f^*} \tag{49}$$

Because the quadratic form in (47) is concave-up, the inequality is satisfied between these roots. Although we can make no angle-rate-dependent restriction on range in this special case, we can still restrict the possible values of range rate using (49).

In the more general case, if $\|\dot{\mathbf{u}}\| \neq 0$ then the roots of the equality (44) are

$$\rho = \frac{1}{(\dot{\mathbf{u}} \cdot \dot{\mathbf{u}})}\left\{-\left(\dot{\mathbf{R}} \cdot \dot{\mathbf{u}}\right) \pm \sqrt{\left(\dot{\mathbf{R}} \cdot \dot{\mathbf{u}}\right)^2 + (\dot{\mathbf{u}} \cdot \dot{\mathbf{u}})\left[\frac{\mu}{a_{MIN}}\left(\frac{1 + e_{MAX}}{1 - e_{MAX}}\right) - f^*\right]}\right\} \tag{50}$$

Real roots for range exist here if and only if the argument of the square root is non-negative:

$$\left(\dot{\mathbf{R}} \cdot \dot{\mathbf{u}}\right)^2 + (\dot{\mathbf{u}} \cdot \dot{\mathbf{u}})\left[\frac{\mu}{a_{MIN}}\left(\frac{1 + e_{MAX}}{1 - e_{MAX}}\right) - f^*\right] \geq 0 \tag{51}$$

$$\frac{\left(\dot{\mathbf{R}} \cdot \dot{\mathbf{u}}\right)^2}{(\dot{\mathbf{u}} \cdot \dot{\mathbf{u}})} + \left[\frac{\mu}{a_{MIN}}\left(\frac{1 + e_{MAX}}{1 - e_{MAX}}\right) - f^*\right] \geq 0 \tag{52}$$

$$f^{**} \leq \frac{\mu}{a_{MIN}}\left(\frac{1 + e_{MAX}}{1 - e_{MAX}}\right) \tag{53}$$

where the quantity f^* is defined as

$$f^{**} = \dot{\mathbf{R}} \cdot \dot{\mathbf{R}} - \left(\dot{\mathbf{R}} \cdot \mathbf{u}\right)^2 - \frac{\left(\dot{\mathbf{R}} \cdot \dot{\mathbf{u}}\right)^2}{(\dot{\mathbf{u}} \cdot \dot{\mathbf{u}})} = f^* - \frac{\left(\dot{\mathbf{R}} \cdot \dot{\mathbf{u}}\right)^2}{(\dot{\mathbf{u}} \cdot \dot{\mathbf{u}})} \tag{54}$$

If the appropriate condition (53) or (46) is not satisfied, then we can eliminate the observation from further consideration and form no hypotheses with it, because no real values for range, and hence for range rate, are possible.

Because we also require that possible values of the range be non-negative, we now examine the conditions under which the real roots given by (50) are non-negative. To do this, we apply Descartes' rule of signs to the equality in (44):

If $\dot{\mathbf{R}} \cdot \dot{\mathbf{u}} > 0$ and $f^* > \frac{\mu}{a_{MIN}}\left(\frac{1+e_{MAX}}{1-e_{MAX}}\right)$, then we have no sign changes and hence no positive real roots. In that case, we can eliminate the observation from further consideration and form no hypotheses with it, because no non-negative values of range can be found that will lead to real values for range rate.

If $\dot{\mathbf{R}} \cdot \dot{\mathbf{u}} > 0$ and $f^* < \frac{\mu}{a_{MIN}}\left(\frac{1+e_{MAX}}{1-e_{MAX}}\right)$, then we have one sign change and hence one positive real root, besides one negative real root. Values of range between 0 and the positive real root will lead to real values of range rate.

If $\dot{\mathbf{R}} \cdot \dot{\mathbf{u}} < 0$ and $f^* < \frac{\mu}{a_{MIN}}\left(\frac{1+e_{MAX}}{1-e_{MAX}}\right)$, then again we have one positive real root, besides one negative real root, so values of range between 0 and the positive root will lead to real values for range rate.

If $\dot{\mathbf{R}} \cdot \dot{\mathbf{u}} < 0$ and $f^* > \frac{\mu}{a_{MIN}}\left(\frac{1+e_{MAX}}{1-e_{MAX}}\right)$, then we have two sign changes and hence two positive real roots. Values of range between these two roots will lead to real values for range rate.

In the special case $\dot{\mathbf{R}} \cdot \dot{\mathbf{u}} = 0$, the roots reduce to

$$\rho = \pm \sqrt{\frac{1}{(\dot{\mathbf{u}} \cdot \dot{\mathbf{u}})} \left[\frac{\mu}{a_{MIN}} \left(\frac{1 + e_{MAX}}{1 - e_{MAX}} \right) - f^* \right]} \tag{55}$$

Hence, real roots are possible in this special case if and only if $f^* < \frac{\mu}{a_{MIN}} \left(\frac{1 + e_{MAX}}{1 - e_{MAX}} \right)$, which produces one positive root, besides one negative root. Values of range between 0 and the positive root will lead to real values for range rate.

In the special case $f^* = \frac{\mu}{a_{MIN}} \left(\frac{1 + e_{MAX}}{1 - e_{MAX}} \right)$, equation (44) reduces to

$$\rho \left(\rho \, \dot{\mathbf{u}} \cdot \dot{\mathbf{u}} + 2 \dot{\mathbf{R}} \cdot \dot{\mathbf{u}} \right) \leq 0 \tag{56}$$

The roots reduce to $\rho = 0$ and $\rho = -2 (\dot{\mathbf{R}} \cdot \dot{\mathbf{u}})/(\dot{\mathbf{u}} \cdot \dot{\mathbf{u}})$, and the inequality is satisfied between these roots. The roots are non-negative only if $\dot{\mathbf{R}} \cdot \dot{\mathbf{u}} \leq 0$. Values of range between 0 and the positive root will lead to real values for range rate.

5.2   Apogee Speed Case

Now we consider the apogee case. Using (37) and (38), we require that

$$\frac{\mu}{a_{MAX}} \left(\frac{1 - e_{MAX}}{1 + e_{MAX}} \right) \leq \dot{\mathbf{R}} \cdot \dot{\mathbf{R}} + 2 \rho \dot{\mathbf{R}} \cdot \mathbf{u} + 2 \rho \dot{\mathbf{R}} \cdot \dot{\mathbf{u}} + \dot{\rho}^2 + \rho^2 \, \dot{\mathbf{u}} \cdot \dot{\mathbf{u}} \tag{57}$$

As in the perigee speed case, to define this region explicitly in terms of one of the variables, we can solve this inequality either for range rate in terms of range or range in terms of range rate, and the results are exactly equivalent, given either choice. Again we choose to solve for range rate in terms of range.

$$\dot{\rho}^2 + 2 \dot{\rho} \dot{\mathbf{R}} \cdot \mathbf{u} + \rho^2 \, \dot{\mathbf{u}} \cdot \dot{\mathbf{u}} + 2 \rho \dot{\mathbf{R}} \cdot \dot{\mathbf{u}} + \dot{\mathbf{R}} \cdot \dot{\mathbf{R}} - \frac{\mu}{a_{MAX}} \left(\frac{1 - e_{MAX}}{1 + e_{MAX}} \right) \geq 0 \tag{58}$$

The roots of the equality are

$$\dot{\rho} = - \dot{\mathbf{R}} \cdot \mathbf{u} \pm \sqrt{ \left(\dot{\mathbf{R}} \cdot \mathbf{u} \right)^2 - \left[\rho^2 \, \dot{\mathbf{u}} \cdot \dot{\mathbf{u}} + 2 \rho \dot{\mathbf{R}} \cdot \dot{\mathbf{u}} + \dot{\mathbf{R}} \cdot \dot{\mathbf{R}} - \frac{\mu}{a_{MAX}} \left(\frac{1 - e_{MAX}}{1 + e_{MAX}} \right) \right] } \tag{59}$$

Provided that we have real roots for range rate, the inequality (58) is satisfied outside the interval between the roots, because the quadratic form is concave-up. However, notice now that if the real roots in (59) are close together, the inequality (58) provides less restriction on the choice of range rate. Here we have essentially the complement of the situation that we had in the perigee case. Let us examine this different situation in detail.

Real roots for range rate as given by (59) exist if and only if the argument of the square root is non-negative:

$$\left(\dot{\mathbf{R}} \cdot \mathbf{u} \right)^2 - \left[\rho^2 \, \dot{\mathbf{u}} \cdot \dot{\mathbf{u}} + 2 \rho \dot{\mathbf{R}} \cdot \dot{\mathbf{u}} + \dot{\mathbf{R}} \cdot \dot{\mathbf{R}} - \frac{\mu}{a_{MAX}} \left(\frac{1 - e_{MAX}}{1 + e_{MAX}} \right) \right] \geq 0 \tag{60}$$

This expression is the same as inequality (43) above, with $\frac{\mu}{a_{MAX}} \left(\frac{1 - e_{MAX}}{1 + e_{MAX}} \right)$ in place of $\frac{\mu}{a_{MIN}} \left(\frac{1 + e_{MAX}}{1 - e_{MAX}} \right)$. Following the same steps as before, we can write (60) in the same form as (44):

$$\rho^2 \, \dot{\mathbf{u}} \cdot \dot{\mathbf{u}} + 2 \rho \dot{\mathbf{R}} \cdot \dot{\mathbf{u}} + \left[f^* - \frac{\mu}{a_{MAX}} \left(\frac{1 - e_{MAX}}{1 + e_{MAX}} \right) \right] \leq 0 \tag{61}$$

If the equality in (61) has no real roots, then no real values of range can be found that will lead to real roots in (59) restricting the choice of range rate. In effect, all real values of range rate satisfy (58). If the equality in (61) has real roots, then the inequality, being concave-up, is satisfied for all values of range between the roots, and these values of range lead to real values of range rate given by (59) above. Consequently, real values for range rate between the roots (59) are excluded from consideration according to the inequality in (58). Of course, we also require that the range be non-negative, which further restricts the values of range rate allowed by (58).

As an aside, we note that, if $\|\dot{\mathbf{u}}\| = 0$, then, independently of the value of range, the inequality (61) reduces to

$$f^* \leq \frac{\mu}{a_{\text{MAX}}} \left(\frac{1 - e_{\text{MAX}}}{1 + e_{\text{MAX}}} \right) \tag{62}$$

Therefore, in the special case of zero total angular rate, all values of range rate are possible if (62) is not satisfied, because, in that case, no real values for range rate result from (59). If the total angular rate is zero, but (62) is satisfied, then the inequality (58) reduces to an expression involving range rate but not range:

$$\dot{\rho}^2 + 2\dot{\rho}\dot{\mathbf{R}} \cdot \mathbf{u} + \dot{\mathbf{R}} \cdot \dot{\mathbf{R}} - \frac{\mu}{a_{\text{MAX}}} \left(\frac{1 - e_{\text{MAX}}}{1 + e_{\text{MAX}}} \right) \geq 0 \tag{63}$$

The roots in this case are real and reduce to

$$\dot{\rho} = - \dot{\mathbf{R}} \cdot \mathbf{u} \pm \sqrt{\left(\dot{\mathbf{R}} \cdot \mathbf{u} \right)^2 - \left[\dot{\mathbf{R}} \cdot \dot{\mathbf{R}} - \frac{\mu}{a_{\text{MAX}}} \left(\frac{1 - e_{\text{MAX}}}{1 + e_{\text{MAX}}} \right) \right]} \tag{64}$$

$$\dot{\rho} = - \dot{\mathbf{R}} \cdot \mathbf{u} \pm \sqrt{\frac{\mu}{a_{\text{MAX}}} \left(\frac{1 - e_{\text{MAX}}}{1 + e_{\text{MAX}}} \right) - f^*} \tag{65}$$

Because the quadratic form in (63) is concave-up, the inequality is satisfied outside these roots. Although we can make no angle-rate-dependent restriction on range in this special case, we can still restrict the possible values of range rate using (65).

In the more general case, if $\|\dot{\mathbf{u}}\| \neq 0$ then the roots of the equality (61) are

$$\rho = \frac{1}{(\dot{\mathbf{u}} \cdot \dot{\mathbf{u}})} \left\{ - \left(\dot{\mathbf{R}} \cdot \dot{\mathbf{u}} \right) \pm \sqrt{\left(\dot{\mathbf{R}} \cdot \dot{\mathbf{u}} \right)^2 + (\dot{\mathbf{u}} \cdot \dot{\mathbf{u}}) \left[\frac{\mu}{a_{\text{MAX}}} \left(\frac{1 - e_{\text{MAX}}}{1 + e_{\text{MAX}}} \right) - f^* \right]} \right\} \tag{66}$$

Real roots for range exist here if and only if the argument of the square root is non-negative:

$$\left(\dot{\mathbf{R}} \cdot \dot{\mathbf{u}} \right)^2 + (\dot{\mathbf{u}} \cdot \dot{\mathbf{u}}) \left[\frac{\mu}{a_{\text{MAX}}} \left(\frac{1 - e_{\text{MAX}}}{1 + e_{\text{MAX}}} \right) - f^* \right] \geq 0 \tag{67}$$

$$\frac{\left(\dot{\mathbf{R}} \cdot \dot{\mathbf{u}} \right)^2}{(\dot{\mathbf{u}} \cdot \dot{\mathbf{u}})} + \left[\frac{\mu}{a_{\text{MAX}}} \left(\frac{1 - e_{\text{MAX}}}{1 + e_{\text{MAX}}} \right) - f^* \right] \geq 0 \tag{68}$$

$$f^{**} \leq \frac{\mu}{a_{\text{MAX}}} \left(\frac{1 - e_{\text{MAX}}}{1 + e_{\text{MAX}}} \right) \tag{69}$$

If the appropriate condition (69) or (62) is not satisfied, then all values of range and range rate are possible.

Because we also require that possible values of the range be non-negative, we now examine the conditions under which the real roots of the equality in (61) are non-negative. To do this, we apply Descartes' rule of signs to that equality:

If $\dot{\mathbf{R}} \cdot \dot{\mathbf{u}} > 0$ and $f^* > \frac{\mu}{a_{\text{MAX}}} \left(\frac{1 - e_{\text{MAX}}}{1 + e_{\text{MAX}}} \right)$, then we have no sign changes and hence no positive real roots. In that case, all values of range rate are possible for positive values of range and the apogee speed condition provides no new information, because no non-negative values of range can be found that will lead to real values for range rate.

If $\dot{\mathbf{R}} \cdot \dot{\mathbf{u}} > 0$ and $f^* < \frac{\mu}{a_{\text{MAX}}} \left(\frac{1 - e_{\text{MAX}}}{1 + e_{\text{MAX}}} \right)$, then we have one sign change and hence one positive real root, besides one negative real root. Values of range between 0 and the positive real root will lead to real values of range rate. All values of range rate are possible for values of range greater than the positive root in (66).

If $\dot{\mathbf{R}} \cdot \dot{\mathbf{u}} < 0$ and $f^* < \frac{\mu}{a_{\text{MAX}}} \left(\frac{1 - e_{\text{MAX}}}{1 + e_{\text{MAX}}} \right)$, then again we have one positive real root, besides one negative real root, so values of range between 0 and the positive root will lead to real values for range rate. All values of range rate are possible for values of range greater than the positive root in (66).

If $\dot{\mathbf{R}} \cdot \dot{\mathbf{u}} < 0$ and $f^* > \frac{\mu}{a_{\text{MAX}}} \left(\frac{1 - e_{\text{MAX}}}{1 + e_{\text{MAX}}} \right)$, then we have two sign changes and hence two positive real roots. Values of range between these two roots will lead to real values for range rate. All values of range rate are possible for values of range between 0 and the smaller positive root in (66) and greater than the larger positive root.

In the special case $\dot{\mathbf{R}} \cdot \dot{\mathbf{u}} = 0$, the roots reduce to a form analogous to (55):

$$\rho = \pm \sqrt{\frac{1}{(\dot{\mathbf{u}} \cdot \dot{\mathbf{u}})} \left[\frac{\mu}{a_{\text{MAX}}} \left(\frac{1 - e_{\text{MAX}}}{1 + e_{\text{MAX}}} \right) - f^* \right]} \tag{70}$$

Hence, real roots are possible in this special case if and only if $f^* < \frac{\mu}{a_{\text{MAX}}} \left(\frac{1 - e_{\text{MAX}}}{1 + e_{\text{MAX}}} \right)$, which produces one positive root, besides one negative root. Values of range between 0 and the positive root will lead to real values for range rate. All values of range rate are possible for values of range greater than the positive root.

In the special case $f^* = \frac{\mu}{a_{\text{MAX}}} \left(\frac{1 - e_{\text{MAX}}}{1 + e_{\text{MAX}}} \right)$, equation (61) reduces to the same form as (56):

$$\rho \left(\rho \, \dot{\mathbf{u}} \cdot \dot{\mathbf{u}} + 2 \dot{\mathbf{R}} \cdot \dot{\mathbf{u}} \right) \geq 0 \tag{71}$$

The roots reduce to $\rho = 0$ and $\rho = -2 (\dot{\mathbf{R}} \cdot \dot{\mathbf{u}}) / (\dot{\mathbf{u}} \cdot \dot{\mathbf{u}})$, and the inequality is satisfied between these roots. The roots are non-negative only if $\dot{\mathbf{R}} \cdot \dot{\mathbf{u}} \leq 0$, in which case values of range between 0 and the positive root will lead to real values for range rate. All values of range rate are possible for values of range greater than the positive root. If $\dot{\mathbf{R}} \cdot \dot{\mathbf{u}} > 0$, all values of range rate are possible for positive values of range and the apogee speed condition provides no new information.

6.   EFFECTS OF ANGLE RATE ERRORS

The importance of using angle rate information, if it is available, was discussed in an earlier section. It remains to be seen, however, how accurate these angle rates need to be to produce reasonable data association hypotheses. Actually, there are two questions which need to be addressed: (i) How accurate do angle rates need to be to represent the orbital state directly? (ii) How accurate do angle rates need to be to reasonably refine our bounds on range for use in a Lambert-based approach? Note that, since our primary purpose is data association, question (i) is not as stressing as it may seem. The reason is that an accurate angles-only IOD can, at least in principle, be obtained once two or more observations has been associated, assuming that the angles themselves are accurate.

Given a line-of-sight observation with right ascension α and declination δ, the observed unit vector in the geocentric inertial frame is

$$\mathbf{u} = \begin{bmatrix} \cos \delta \cos \alpha \\ \cos \delta \sin \alpha \\ \sin \delta \end{bmatrix} \tag{72}$$

Differentiating with respect to time, we get

$$\dot{\mathbf{u}} = \dot{\delta} \begin{bmatrix} -\sin \delta \cos \alpha \\ -\sin \delta \sin \alpha \\ \cos \delta \end{bmatrix} + \dot{\alpha} \begin{bmatrix} -\cos \delta \sin \alpha \\ \cos \delta \cos \alpha \\ 0 \end{bmatrix} \tag{73}$$

in which the angle rates $\dot{\alpha}$ and $\dot{\delta}$ appear linearly. Recall from (36) that $\dot{\mathbf{u}}$ appears linearly in the expression for $\dot{\mathbf{r}}$. (Angle rate errors have no effect on $\mathbf{r}$.) Therefore, errors in the angle rates $\dot{\alpha}$ and $\dot{\delta}$ are transformed linearly into orbit velocity errors. This means that, for example, if the angle rate errors are Gaussian, they will produce Gaussian

errors in orbit velocity. To answer question (i), it is thus relatively straightforward to select maximum permissible angle rate errors for a given problem based on maximum permissible errors in orbit velocity.

To investigate the effect of angle rate errors on the range, range rate bounds defined in the previous section, we first examine the roots of inequalities (41) and (58), given by equations (42) and (59), respectively, both of which have exactly the same form. Since $\dot{\mathbf{u}}$ appears only inside the radical in these equations, we can conclude that, for a given value of range, angle rate errors will either stretch or compress the interval of range rate values defined by the inequality but will not change the mean of this interval since it is symmetric about the unaffected value $(-\dot{\mathbf{R}} \cdot \mathbf{u})$ in both cases. Angle rate errors will also affect the intervals of range values, given by (44) and (61), yielding real range rate roots. The roots of these range inequalities are given by equations (50) and (66): this time $\dot{\mathbf{u}}$ affects both the center and width of these intervals.

Thus, the effect of angle rate errors on our range, range rate bounds is to distort them by stretching or compressing about $(-\dot{\mathbf{R}} \cdot \mathbf{u})$ in the range rate direction and by stretching, compressing, and translating them in the range direction. For a given magnitude of expected angle rate errors, this distortion can be accounted for by padding the range, range rate bounds by an amount sufficient to guarantee that the resulting hypothesis region still contains the true admissible region. The amount of padding required depends on specific observation geometry and could be computed either on a case by case basis or conservatively in a worst case sense using an appropriate stressing geometry. It is worth noting that, since our method already produces conservative bounds, we are already somewhat protected from small angle rate errors. However, although none of our simulations so far have produced results in which the admissible region lies very close to the explicit bounds, we have no guarantee of this, so it will still be important to account for even small angle rate errors when using this method.

7. NUMERICAL EXAMPLE

The results of the previous sections are illustrated for a pair of simulated observations of a space object undergoing unperturbed Keplerian motion. This example treats the case of simultaneous observation of angles and angle rates since the use of both of these data types offers an opportunity for reduction in complexity of the problem compared to using angle data alone. The orbit plane bounds are not applied in this example. Table 1 lists the relevant position, velocity and orbit quantities of the system, and Table 2 lists the element partitions used.

Table 2. Orbital and Observational Data

Quantity	Value
$\mathbf{R}_1$	[4092, 2690, 4076] km
$\mathbf{R}_2$	[3971, 2866, 4076] km
$\dot{\mathbf{R}}_1$	[-0.196, 0.298, 0] km/sec
$\dot{\mathbf{R}}_2$	[-0.209, 0.290, 0] km/sec
$\mathbf{r}_1$	[8102, 2576, 5271] km
$\mathbf{r}_2$	[5977, 5560, 6548] km
$\dot{\mathbf{r}}_1$	[-2.683, 5.383, 2.786] km/sec
$\dot{\mathbf{r}}_2$	[-4.282, 4.470, 1.452] km/sec
(ρ_1, ρ_2)	(4185, 4170) km
$(\dot{\rho}_1, \dot{\rho}_2)$	(-1.724, 1.600) km/sec
$t_2 - t_1$	600 sec
a	11149 km
e	0.145

Table 1. Element Partition

Element	Partition (min, max)
a	(11049, 11249) km
e	(0.12, 0.1555)

For perfect angles and angle rates, the range, range rate hypothesis region based on the maximum perigee and minimum apogee speed conditions is shown for each observation in Fig. 3 and 4, along with the angles-only range bounds, admissible region (determined by solving the orbit problem for each range, range rate hypothesis pair and checking the resulting a and e values), and actual values of ρ and $\dot{\rho}$. As discussed in the previous section, when angle rate errors are applied, the hypothesis region is distorted by some amount, but the angles-only range bounds are unaffected. In particular, if angle rate errors are expected to be large enough to make for a questionable orbit solution, they can still be used to refine the range, range hypothesis region for use in a Lambert-based method (in which case only the perigee speed condition needs to be evaluated, since the apogee speed condition is valid for at least some values of range rate for all possible values of range). This situation is shown in Fig. 5, with the range, range hypothesis region plotted alongside the angle-rate-implied range bounds (with and without errors), range, range admissible region (determined by solving the Lambert problem for each range hypothesis pair), and actual values of ρ_1 and ρ_2. The thin red lines show the amount of padding required
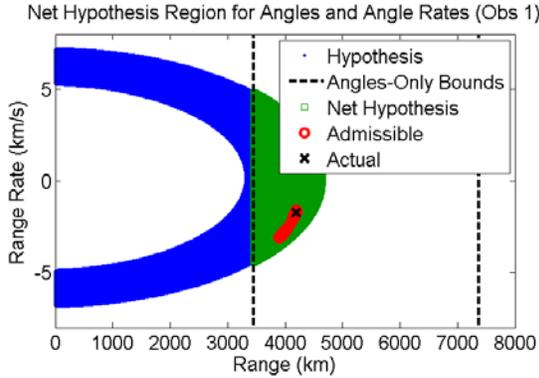
Fig. 5. Observation 1 with perfect data.
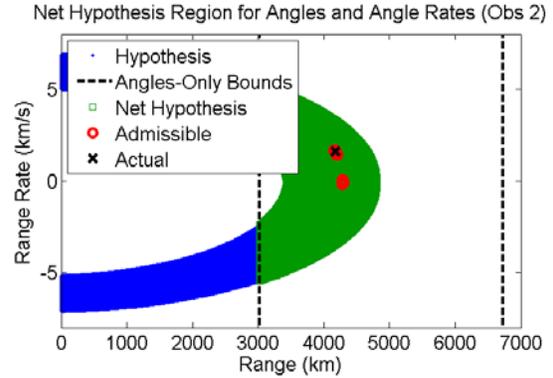
Fig. 4. Observation 2 with perfect data.

for the angle-rate-implied range bounds to account for expected ±1 or ±3 arcsecond/sec errors in both $\dot{\alpha}$ and $\dot{\delta}$. Padding the bounds by these amounts guarantees that the net hypothesis region will contain the admissible region, but the number of Lambert solutions required will still be greatly reduced.

Once admissible candidate orbits have been generated, by evaluating range, range rate hypothesis pairs (or range hypothesis pairs, in the Lambert-based case), the next step is to address the data association problem. This is by no means a trivial matter, as it involves comparing two six-dimensional random vectors and evaluating some kind of "distance" metric between them. A detailed treatment of this subject is beyond the present work, but we will show *ad hoc* results to illustrate how an appropriate method could be effective.

The classical orbital elements for each candidate orbit lying inside the range, range rate admissible regions for observations 1 and 2 are shown in Fig. 6–8. Examining the candidate a and e pairs first, in Fig. 6, note that the spacing of the values is not uniform. This is a consequence of our using a rectangular grid to sample the range, range rate space, which does not correspond to a rectangular grid in orbital element space. This may represent an inefficiency to the method which could be addressed by adopting an alternate sampling method, such as one of those suggested by Tommei et al. [13] or Siminski et al. [21,22]. Examining the remaining elements i, Ω, ω, and M_0, in Fig. 7 and 8, it is clear that the candidate orbital elements overlap in a unique region. The intersection is particularly clear for the elements i and Ω, in Fig. 7. The "association hypothesis region" is then defined by taking a small region around the intersection of the two six-dimensional admissible candidate orbit regions. In this example, the region is found by comparing the candidate orbits pairwise and retaining those whose six orbital elements all lie within some small tolerance of one another. If no association hypotheses result from this comparison then the two observations are not associated with the same space object.
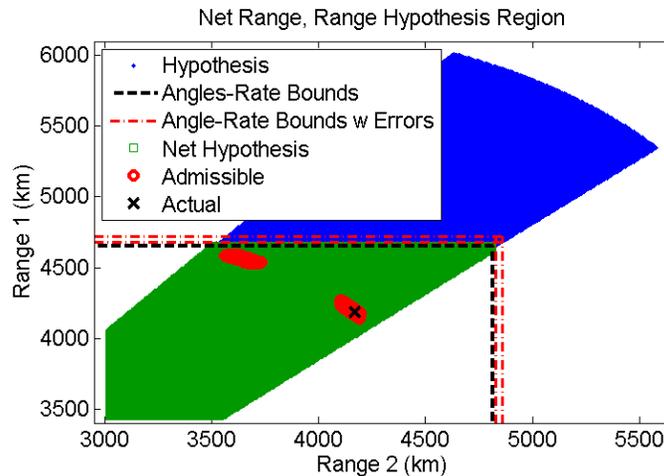
Fig. 3. Range, range hypothesis region with angle rate errors.
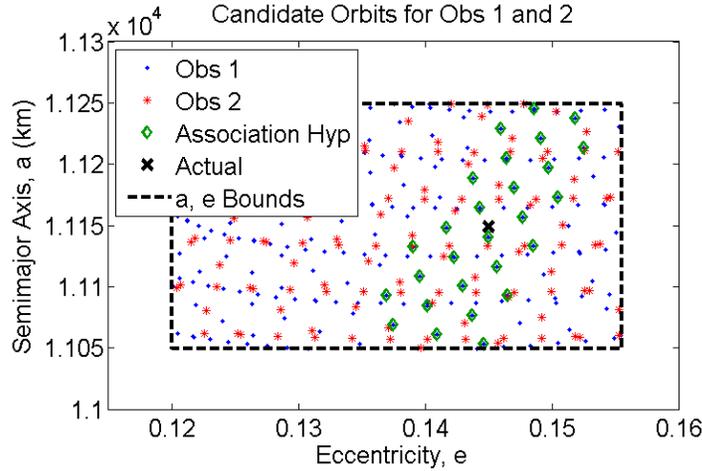
Fig. 8. Candidate a and e pairs for each observation.

As mentioned in the previous section, even if angle rate errors are large enough that they cannot be relied upon to produce an accurate IOD, they may still be useful for solving the data association problem. For example, angle rates could be used to generate admissible candidate orbits, as just described, which could then be compared for a pair of observations. If the six-dimensional admissible candidate orbit regions intersect, or, more generally, if they lie sufficiently "close" to one another (a concept which is left deliberately vague in the present paper), then the observations are possibly associated and a set of accurate candidate IODs can be obtained using a Lambert-based approach. A very efficient catalog-building algorithm could be designed in such a way, employing increasingly complex orbit determination methods as the number of hypotheses are reduced by filter steps along the way.

8.   SUMMARY AND CONCLUSION

Our results show that the possible values of range and range rate can be limited *a priori* for each line-of-sight observation to finite intervals corresponding to a specified partition of the element space. The endpoints of the intervals are given explicitly in terms of the angle-based observations, station position and station velocity, and can be computed independently for each observation. In the angles-only case, additional conditions based on special solutions of Lambert's problem, which must be satisfied by range values for pairs of observations, can be used to further reduce the number of Lambert solutions needed for the initial orbit determinations (IODs). We also investigate the problem of angle rate errors and their effect on both the IOD and the range, range rate bounds, and we provide methods for dealing with this issue in both of these cases. All of the formulas derived here apply uniformly to Earth-bound and space-based observing stations. We also describe explicit conditions identifying when a given observation does not correspond to any possible orbit within the specified element-space partition. Such observations can be discarded before any data association hypotheses or orbit solutions are produced.
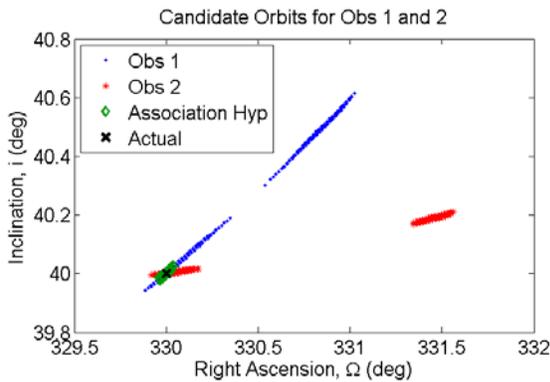
Fig. 7. Candidate i and Ω pairs.
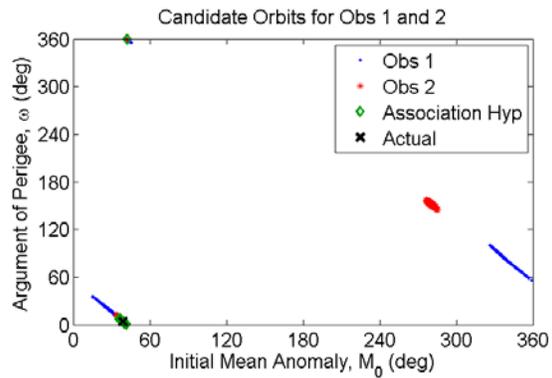
Fig. 6. Candidate ω and M_0 pairs.

Using this approach, the computational complexity of the track initiation job for N line-of-sight observations decreases from N^3 (or more) for traditional range-solution methods to $N^2 M^2$, where M is the number of range hypotheses assigned to each observation. If accurate angle rates are available, the computational further decreases to NML, where L is the number of range rate hypotheses assigned to each observation. Introducing element partitions also makes the problem embarrassingly parallelizable, so that we can keep the number of range and range rate hypotheses for each partition manageable in principle simply by making the partitions smaller and using more processors.

The range and range rate bounds described in this paper allow a convenient parallelization of the task of computing initial orbits in large space surveillance tracking scenarios, which is the phase of the tracking job that involves most of the computational complexity. Because the bounds are conservative to some extent and not exact, some values of range and range rate that lie within the bounds given here will lead to candidate orbits that lie outside the specified partition of the element space. This fact leads to some inefficiency in the parallelization of the initial orbit hypotheses over the whole element space. Essentially, nearly duplicated candidate orbits may be generated near the boundaries of the specified partitions and would therefore have to be identified and merged later in the tracking process. Although the detection and merging of duplicate tracks must always be done in any multiple-hypothesis tracking implementation, the inefficiency of our range and range rate bounds necessarily increases the size of that task. The actual cost of this inefficiency in particular problems will depend on the observation sets, the element partitions of interest and the range, range rate sampling strategy, and may need to be studied if the scenario is computationally stressing. On the other hand, all the orbits within an element-space partition correspond to values of range and range rate that do lie within the bounds given here, so that no candidate orbits will be missed merely through this choice of bounds.

9. REFERENCES

[1] S. L. Coffey, E. Jenkins, H. L. Neal, and H. Reynolds, "Parallel Processing of Uncorrelated Observations into Satellite Orbits," *Advances in the Astronautical Sciences*, Vol. 93, 1996, pp. 739–756. (Proceedings of the 6th AAS/AIAA Space Flight Mechanics Conference, February 12–15 1996, Austin, Texas).

[2] S. L. Coffey, L. M. Healy, and H. L. Neal, "Applications of Parallel Processing to Astrodynamics," *Celestial Mechanics and Dynamical Astronomy*, Vol. 66, No. 1, 1996, pp. 61–70.

[3] S. L. Coffey, H. L. Neal, and M. M. Berry, "Uncorrelated Observations Processing at Naval Space Command," *Journal of Guidance, Control, and Dynamics*, Vol. 25, July–August 2002, pp. 676–684.

[4] P. R. Escobal, *Methods of Orbit Determination*. John Wiley & Sons, Inc., 1965. (Reprint with corrections by Krieger Publishing Company, 1976).

[5] R. H. Gooding, "A New Procedure for Orbit Determination Based on Three Lines of Sight (Angles Only)," Defense Research Agency Technical Report 93004, Farnborough, Hampshire, GU14 6TD, United Kingdom, 13 April 1993. Available through Defense Technical Information Center and National Technical Information Service (USA).

[6] R. H. Gooding, "A New Procedure for the Solution of the Classical Problem of Minimal Orbit Determination from Three Lines of Sight," *Celestial Mechanics and Dynamical Astronomy*, Vol. 66, No. 4, 1997, pp. 387–423.

[7] R. R. Karimi and D. Mortari, "Initial Orbit Determination using Multiple Observations," *Celestial Mechanics and Dynamical Astronomy*, Vol. 109, No. 2, 2011, pp. 167–180.

[8] A. J. Sarnecki, "A Projective Approach to Orbit Determination from Three Sight Lines," *Celestial Mechanics and Dynamical Astronomy*, Vol. 66, No. 4, 1997, pp. 425–451.

[9] K. J. DeMars, M. K. Jah, and P. W. Schumacher, Jr., "The Use of Angle and Angle Rate Data for Deep-Space Orbit Determination and Track Association," *Advances in the Astronautical Sciences*, Vol. 136, 2010. (Proceedings of the 20th AAS/AIAA Space Flight Mechanics Conference, San Diego, California, February 14–17 2010).

[10] K. J. DeMars, M. K. Jah, and P. W. Schumacher, Jr., "Initial Orbit Determination using Short-Arc Angle and Angle Rate Data," *IEEE Transactions on Aerospace and Electronic Systems*, Vol. 43, No. 3, pp. 2628–2637.

[11] A. Milani, G. F. Gronchi, M. D. Vitturi, and Z. Knezevic, "Orbit Determination with Very Short Arcs: I. Admissible Regions," *Celestial Mechanics and Dynamical Astronomy*, Vol. 90, 2004, pp. 59–87.

[12] A. Milani and Z. Knezevic, "From Astrometry to Celestial Mechanics: Orbit Determination with Very Short Arcs," *Celestial Mechanics and Dynamical Astronomy*, Vol. 92, 2005, pp. 1–18.

[13] G. Tommei, A. Milani, and A. Rossi, "Orbit Determination of Space Debris: Admissible Regions," *Celestial Mechanics and Dynamical Astronomy*, Vol. 97, 2007, pp. 289–304.

[14] G. Tommei, A. Milani, D. Farnocchia, and A. Rossi, "Correlation of Space Debris Observations by the Virtual Debris Algorithm," *Proceedings of the Fifth European Conference on Space Debris*, European Space Operations Center, Darmstadt, Germany, March 30–April 2 2009.

[15] K. Fujimoto, J. M. Maruskin, and D. J. Scheeres, "Circular and Zero-Inclination Solutions for Optical Observations of Earth-Orbiting Objects," *Celestial Mechanics and Dynamical Astronomy*, Vol. 106, 2010, pp. 157–182.

[16] D. Farnocchia, G. Tommei, A. Milani, and A. Rossi, "Innovative Methods of Correlation and Orbit Determination for Space Debris," *Celestial Mechanics and Dynamical Astronomy*, Vol. 107, 2010, pp. 169–185.

[17] G. F. Gronchi, L. Dimare, and A. Milani, "Orbit Determination with the Two-Body Integrals," *Celestial Mechanics and Dynamical Astronomy*, Vol. 107, 2010, pp. 299–318.

[18] K. J. DeMars, M. K. Jah, "Initial Orbit Determination via Gaussian Mixture Approximation of the Admissible Region," *Advances in the Astronautical Sciences*, Vol. 143, 2012. (Proceedings of the 22nd AAS/AIAA Space Flight Mechanics Conference, Charleston, South Carolina, January 29–February 2 2012).

[19] J. M. Maruskin, D. J. Scheeres, and K. T. Alfriend, "Correlation of Optical Observations of Objects in Earth Orbit," *Journal of Guidance, Control, and Dynamics*, Vol. 32, January–February 2009, pp. 194–209.

[20] A. Milani, G. Tommei, D. Farnocchia, A. Rossi, T. Schildknecht, and R. Jehn, "Correlation and Orbit Determination of Space Objects based on Sparse Optical Data," *Monthly Notices of the Royal Astronomical Society*, Vol. 417, No. 3, 2011, pp. 2094–2103.

[21] J. A. Siminski, O. Montenbruck, H. Fiedler, and M. Weigel, "Best Hypotheses Search on Iso-Energy-Grid for Initial Orbit Determination and Track Association," 23rd AAS/AIAA Spaceflight Mechanics Conference, Kauai, Hawaii, February 10–14 2013.

[22] J. A. Siminski, H. Fiedler, and T. Schildknecht, "Track Association Performance of the Best Hypotheses Search Method," *Proceedings of the Sixth European Conference on Space Debris*, European Space Operations Center, Darmstadt, Germany, April 22–25 2013.